Journal Name

COMMUNICATION

Glycan Shields for Penetrating Peptides

Ivan Gallego & Javier Montenegro[a]*

Received 00th January 20xx,

Accepted 00th January 20xx

DOI: 10.1039/x0xx00000x

www.rsc.org/

We here describe the synthesis and biological evaluation of glycan shields for cell penetrating peptides. A new benzyl alkoxyamine connector was employed for the coupling of two saccharides units in the lateral side chain of individual amino acids in a peptide sequence. The oxyme bond formation with the corresponding glycan aldehydes allowed the preparation of highly glycosylated penetrating peptides with a minimal synthetic effort. Surprisingly, it was found that a four to six saccharide substitution did not decrease uptake efficiency in cells, whereas it significantly improved the toxicity profile of the penetrating peptide. In particular, glucose substitution was confirmed as an optimal glycan shield that showed an excellent *in vitro* uptake and intracellular localization as well as a superior *in vivo* biodistribution.

Over the last years, cell penetrating peptides have attracted great interest due to their enhanced membrane translocation capacities for different molecular and macromolecular cargos.[1–3] The broad range of currently known penetrating peptides sequences still hinders an accurate general description of their internalization mechanism.[4,5] Nevertheless, it is well known that peptide sequences including a certain number of cationic and/or hydrophobic amino acids could present membrane penetrating properties.[6] Under certain experimental conditions, it has been validated that the cationic amphiphilic character drives penetrating peptides across model membranes and inside cells by following a Le Châtelier counterion exchange equilibrium.[7] However, cationic amphiphilicity can also be often associated to toxicity issues related to the non-selective membrane disruption and the binding to anionic biopolymers (e.g., heparin).[6,8] Therefore, different strategies, such as stimuli responsive connectors or transient dynamic helicity, have been developed to minimize the impact of penetrating peptides amphiphilicity.[9–17] Despite the high success of glycosylation strategies for improving the selectivity of different membrane targeted and antimicrobial peptides,[18–20] this approach has been barely explored for cell penetrating peptides.[21–23] This is in part due to the important impact of glycosylation in the internalization efficiency of penetrating peptides. As identified in previous studies by others and us,[21,23,24] the increase in the hydrophilic character that accompanies the introduction of glycan units hinders the efficient membranes interaction and the subsequent translocation of glycosylated penetrating peptides. Thus, the improvement in the toxicity profile by glycan insertion comes at the expense of a strong reduction in the penetration capacity of the peptide carrier.

We here describe a new strategy to multiply the number of glycans pendants in each amino acid of a peptide sequence by using a double alkoxyamine connector for the straightforward oxyme insertion of glycan aldehydes. Three different glycan units, namely glucose, galactose and mannose, were coupled to a penetrating peptide sequence including 6 positively charged arginine residues and 5 hydrophobic leucine side chains (Fig. 1). Monosaccharides were selected for their simplicity and biocompatibility and had been extensively used in the development of glycosylated drug-delivery systems.[25] Surprisingly, it was found that the differences in uptake efficiency observed for the glycosylation increase from 4 to 6 saccharide units were minimal and within the concentration range of a prototypical octa-arginine penetrating peptide control. More importantly, while cytometry uptake evaluation showed similar uptake efficiency, a strong improvement in viability toxicity of the peptide was achieved for the hexa-glycan substituted peptides. In particular, the *in vitro* and *in vivo* characterization of the different glycans tested, confirmed that a coverage of six glucoses residues was an optimal glycan shield for this penetrating peptide. These results support the potential of high-density glycan functionalization, and in particular glucose insertion, for the improvement of the uptake/toxicity profile of short cell penetrating peptides.

Design and synthesis. For the introduction of a high-density glycan shield, a 1,3,5-trisubstituted benzyl alkoxyamine connector was synthesized (Fig. 1d (grey) and Fig. S1). The commercially available methyl 3,5-diaminobenzoate was coupled by amide formation reaction with the (Boc-aminooxy)acetic acid to afford a di-alkoxyamine intermediate, which was then treated with lithium hydroxide to hydrolyse the ester group and yield the final Boc-protected benzyl connector (**1**, Fig. S1). The penetrating peptides of this study Tm**P**$(X)_z$, where X stands for the different glycan moiety (Fig. 1), were synthesized by an Fmoc solid phase strategy[26–28] and methyltrityl (Mtt) protected lysines were employed for the selective deprotection, under weakly acidic conditions and

[a] Centro Singular de Investigación en Química Biolóxica e Materiais Moleculares (CIQUS), Departamento de Química Orgánica, Universidade de Santiago de Compostela, 15782 Santiago de Compostela, Spain. *e-mail: javier.montenegro@usc.es

Electronic Supplementary Information (ESI) available: [details of any supplementary information available should be included here]. See DOI: 10.1039/x0xx00000x.

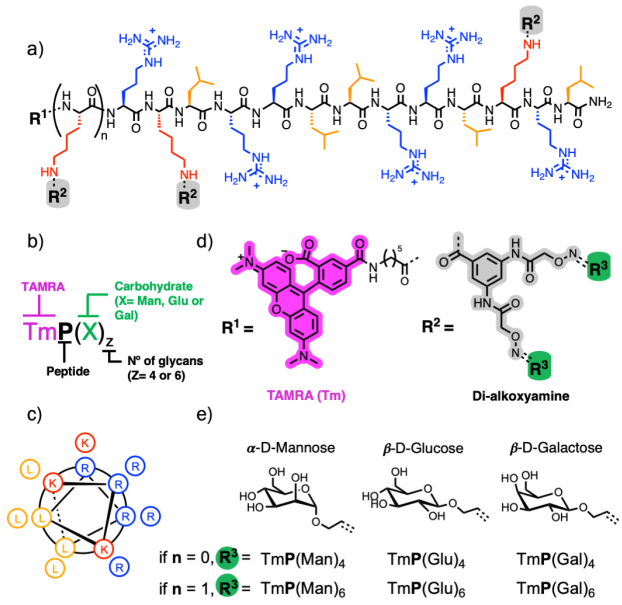

Fig. 1. a) Linear peptide structure with amino acid side chains in colors: cationic arginines (R) in blue, hydrophobic leucines (L) in orange, and modified lysine residues (K-R^2) in red. b) Glycopeptide nomenclature: Tm**P**(X)z, where X corresponds to the type of carbohydrate (X = Man, Glu or Gal) and Z to the number of glycans (Z = 4 or 6). c) Heptad-based wheel diagram for the helical conformation of the peptide. d) The peptides are fluorescently labeled at the *N*-terminus: R^1 substituent TAMRA (Tm). The R^2 substituent anchored to the lysines corresponds to the new benzyl alkoxyamine linker for two R^3 oxime-linkages. e) The R^3 substituents are oxime derivatives of α-D-mannose (Man), β-D-glucose (Glu) and β-D-galactose (Gal). Depending on whether the peptide structure contains two (n = 0) or three lysines (n = 1), the final structure will acquire on its surface 4 or 6 carbohydrate ligands.

and subsequent "*on resin*" coupling with the alkoxyamine benzene connector (Fig. S8). Peptides were N-terminated with a fluorescent probe (TAMRA), cleaved from the solid support (TFA) and, after a previous purification step, conjugated with different glycans aldehydes (see supporting information).[23,29,30] The oxyme bio-orthogonal conjugation proceeded in water at room temperature, in short times and with quantitative yields, allowing the introduction of two saccharide units per single amino acid lateral side chain (Fig. S9). The HPLC purified glycopeptides were characterized by mass spectrometry (MS), ^{1}H-NMR and circular dichroism (CD). The circular dichroism of the different glycopeptides showed the typical α-helix profile,[23] which suggested that the introduction of a high-density glycan shield would not have significant impact in the peptides secondary structure (Fig. S10).

***In vitro* cellular internalization studies**. An *in vitro* evaluation in cells was initially carried out for the four to six saccharide equipped peptides (Fig. 2). Peptides were incubated with HeLa cells for 30 minutes and the cells were thoroughly washed with a heparin-containing solution to remove the excess peptide (see supporting information). The uptake efficiency and the intracellular distribution were then analysed by flow cytometry and confocal microscopy, respectively (Fig. 2). As expected, in the mannose (Tm**P**$(Man)_{4,6}$) and the galactose (Tm**P**$(Gal)_{4,6}$) derivatives, the confocal micrographs already suggested a slight decrease of the total fluorescence signal with the increase in the number of glycans, from the tetra– to hexa–substituted peptides (Fig. 2a). However, a similar signal intensity independent on the number of glycans was observed for the glucose derivate, which also showed a stronger diffuse cytosolic signal for hexa–glucose shielded peptide (Tm**P**$(Glu)_6$) than that of the tetra–substituted (Tm**P**$(Glu)_4$) analogue (Fig. 2a). These results for the hexa–glucose derivative were not expected, as an increase in two hydrophilic glycan residues should, in principle, reduce membrane interaction and cellular internalization. Nevertheless, this trend was confirmed by flow cytometry uptake analysis (Fig. 2b), which validated the expected decrease of uptake for the hexa–mannose and galactose– equipped peptides, but as suggested by confocal micrographs, the cytometry analysis confirmed the counterintuitive uptake increase of the glucose modified peptide (Tm**P**$(Glu)_6$, Fig. 2b). As previously described,[31] the intracellular distribution was concentration-dependent (Fig. 2a), but a similar cytosolic signal for the Tm**P**$(Glu)_6$ and the Tm$\mathbf{R_8}$ control peptide was observed at 5 μM (Fig. S11).

Cytotoxicity studies by mitochondrial metabolic activity analysis were next carried out by following the reduction of the yellow dye 3-(4,5-dimethylthiazol-2-yl)-2,5-diphenyltetrazolium bromide to the purple formazan (MTT colorimetric assay). In contrast to the total uptake efficiency, cytotoxicity studies indicated that the number of glycans did have a strong impact in the toxicity profile of the penetrating peptides (Fig. 2c). In all three cases (Glucose, Mannose, Galactose), the six glycan modified peptides showed a clear reduced toxicity compared to the tetra substituted peptides, specially at high concentrations (Fig. 2c). Despite the minor impact in the internalization efficiency and the intriguing diffuse intracellular localization of the hexa–glucose shielded peptide Tm**P**$(Glu)_6$, this derivative also showed an excellent viability profile with minimal apparent toxicity in all the concentration range employed (1-50 μM, Fig. 2c). These results suggested that optimization of the number and chemical nature of glycan residues could significantly affect and improve the toxicity profile of penetrating peptides without compromising uptake efficiency. A prototypical Tm$\mathbf{R_8}$ octa-arginine penetrating peptide control was employed to calibrate the uptake of glycan shielded peptides. These control experiments showed a slightly decrease uptake efficiency but a strongly improved toxic profile, in the similar concentration range, for the three glycan shielded peptides (Fig. 2b-c and S11). Further control experiments with the acetone capped peptide Tm**P**$(Acetone)_2$ showed a stronger toxicity, even at the low micromolar range, which confirmed the importance of the glycan residues to balance the potential toxicity of amphiphilic penetrating peptides (Fig. S11).

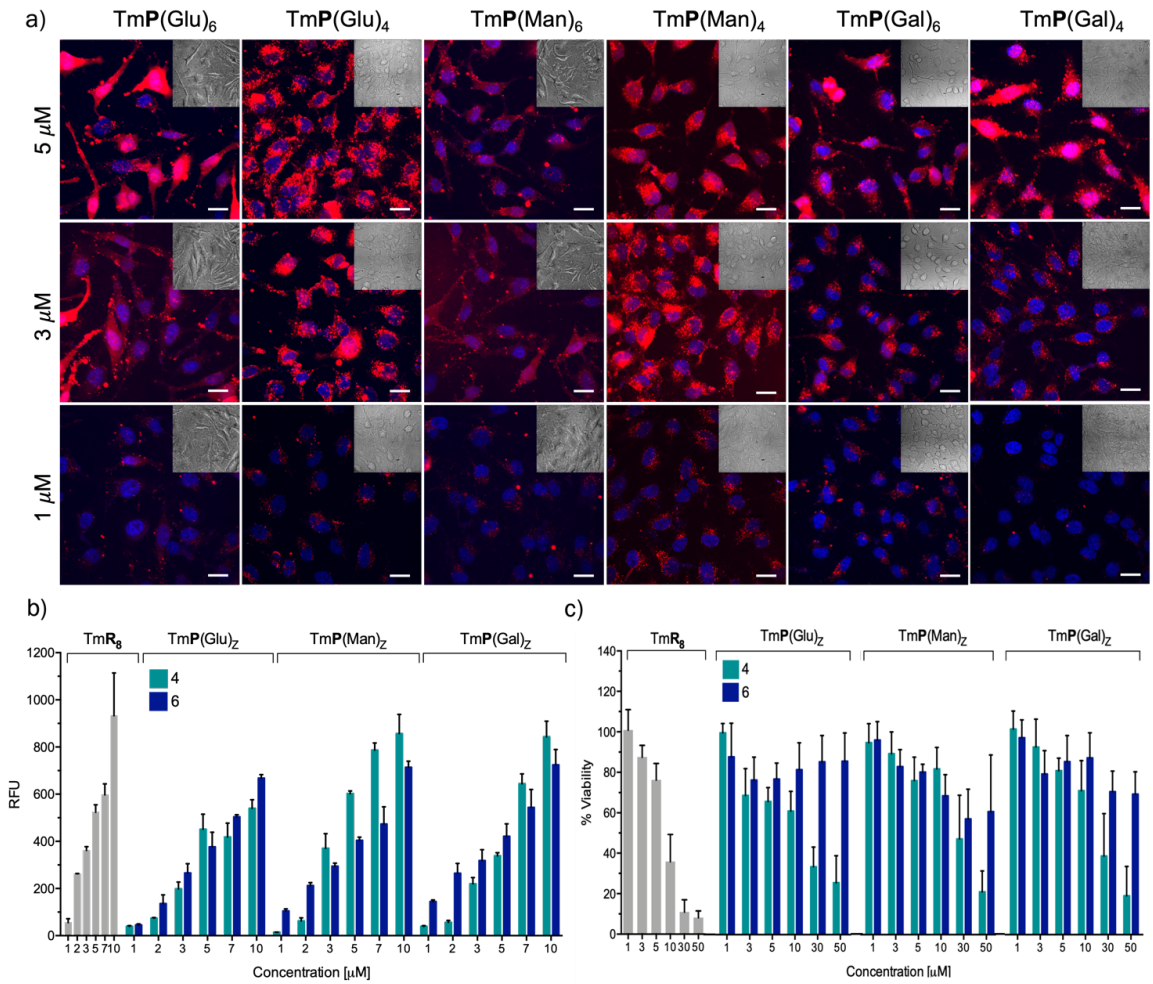

Fig. 2. *In vitro* intracellular distribution and cytotoxicity in HeLa cells. a) Live cell confocal micrographs of glycopeptides at 1, 3 and 5 μM. Columns correspond to glycopeptides and rows to the concentrations. Glycopeptides were incubated in HKR buffer for 30 min at 37°C (see ESI). Glycopeptides (TAMRA) in red, nuclei (Hoechst) in blue, brightfield images on insets. Scale bars: 25 μm. b) Internalization efficiency (1, 2, 3, 5, 7 and 10 μM) by flow cytometry of glycostructures and the control Tm**R**$_8$. c) MTT assay: cytotoxicity of each of the glycopeptides (tetra and hexa saccharides in green and blue respectively) and the control Tm**R**$_8$ (grey) in HeLa cells ((1, 3, 5, 10, 30 and 50 μM)). The data in the graphs are grouped according to carbohydrate ligand (Glu, Man or Gal), where Z = 4 (green) or 6 (blue). Viability of HeLa cells incubated with 5 μM of Tm**P**(Acetone)$_2$ was 17.4% ± 3.6 (Fig. S11). In b) and c) data are presented as the average of three replicates ± standard deviation.

***In vivo* studies**. Prompted by the excellent toxicity profile of high-density glycosylation, an *in vivo* model was carried out to study and compare the potential biodistribution of the hexa–saccharides peptides (Fig. 3). Biodistribution studies in mice were carried out by intravenous injection (tail vein) of solutions of the glycan shielded penetrating peptides in PBS and *in vivo* fluorescence images (IVIS imaging) were acquired after 1hour post-injection (Fig. 3a). Consistent with the *in vitro* results, the fluorescence intensity map indicated an improved biodistribution for the glucose shielded peptide (Tm**P**(Glu)$_6$, Fig. 3b). Endpoint (3 h) *ex vivo* tissue fluorescence quantification (lungs, heart, liver, kidneys and spleen) further confirmed an enhanced fluorescence signal and the capacity to more efficiently reach the lung tissue for the hexa–glucose derivative (Fig. 3b and Fig. S12). Despite minor deviations in the average values for the Galactose derivative (Tm**P**(Gal)$_6$), no traces of toxicity could also be detected from the hematological and biochemical analysis of the corresponding mice treated with the Mannose (Tm**P**(Man)$_6$) and the Glucose (Tm**P**(Glu)$_6$) shielded peptides (Fig. S13-14).

In summary, high-density glycan shields have been incorporated into short penetrating peptide sequences by employing a benzyl alkoxyamine connector to duplicate the number of artificial glycan residues per amino acid in the peptide sequence. The resulting glycosylated peptides showed a comparable internalization rate and a strong improvement in the toxicity profile as compared to a prototypical octa–arginine control. For the different peptide sequences studied, an increase from 4 to 6 glycan surrogates did not strongly reduce the internalization efficiency, and for the glucose derivative, it even increased peptide uptake (Fig. 2b).

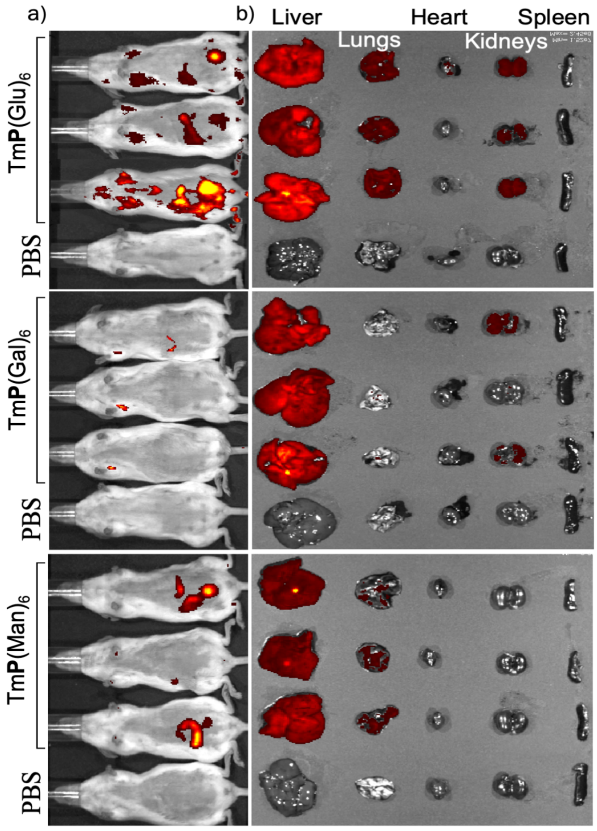

Fig. 3. In vivo biodistribution of TmP(X)$_6$, where X = Glu, Gal or Man. a) *In vivo* images after 1h after intravenous injection of 50 µg of glycopeptides in 50 µL of PBS. A fourth mouse as a control injected with only PBS. b) *Ex vivo* study 3h post-injection and observation of fluorescence for each glycosylated peptide in the different

Confocal microscopy and flow cytometry confirmed the superior properties of the glucose shield in terms of *in vitro* intracellular localization and peptide uptake as well as biodistribution in mice models. These results validate the glucose shield in terms of *in vitro* intracellular localization and total peptide uptake as well as biodistribution for *in vivo* mice models. The results reported here support the application of glycan shields and in particular, high density glucose substitution, to improve the toxicity profile of penetrating peptides with minimal impact in uptake efficiency.

Acknowledgements

Spanish Agencia Estatal de Investigación (AEI) [SAF2017-89890-R, PCI2019-103400, PID2020-117143RB-I00], Xunta de Galicia (ED431C 2017/25, ED431G 2019/03) and the ERDF. J.M. thanks the ERC-Stg (DYNAP, 677786), ISCIII (COV20/00297), ERC-POC (TraffikGene, 838002), Xunta de Galicia (Oportunius Program) and Human Frontier Science Programme Young Investigator Grant (RGY0066/2017) for funding. I.G. received predoctoral fellowships (ED481A-2018/116 and FPU17/00941).

References

1 E. G. Stanzl, B. M. Trantow, J. R. Vargas and P. A. Wender, *Acc. Chem. Res.*, 2013, **46**, 2944–2954.
2 P. Zhang, G. da Silva, C. Deatherage, C. Burd and D. DiMaio, *Cell*, 2018, **174**, 1465–1476.e13.
3 I. Lostalé-Seijo and J. Montenegro, *Nat. Rev. Chem.*, 2018, **2**, 258–277.
4 W. B. Kauffman, T. Fuselier, J. He and W. C. Wimley, *Trends Biochem. Sci.*, 2015, **40**, 749–764.
5 A. Méndez-Ardoy, I. Lostalé-Seijo and J. Montenegro, *ChemBioChem*, 2019, **20**, 488–498.
6 P. M. Fischer, *Med. Res. Rev.*, 2007, **27**, 755–795.
7 G. Gasparini, E.-K. Bang, J. Montenegro and S. Matile, *Chem. Commun.*, 2015, **51**, 10389–10402.
8 D. Kalafatovic and E. Giralt, *Molecules*, 2017, **22**, 1929.
9 Y.-L. Lin, G. Jiang, L. K. Birrell and M. E. H. El-Sayed, *Biomaterials*, 2010, **31**, 7150–7166.
10 C. J. McKinlay, J. R. Vargas, T. R. Blake, J. W. Hardy, M. Kanada, C. H. Contag, P. A. Wender and R. M. Waymouth, *Proc. Natl. Acad. Sci.*, 2017, **114**, E448–E456.
11 Y. Shi, Y. Hu, G. Ochbaum, R. Lin, R. Bitton, H. Cui and H. S. Azevedo, *Chem. Commun.*, 2017, **53**, 7037–7040.
12 S. A. Bode, S. B. P. E. Timmermans, S. Eising, S. P. W. Van Gemert, K. M. Bonger and D. W. P. M. Löwik, *Chem. Sci.*, 2019, **10**, 701–705.
13 S. Ulrich, *Acc. Chem. Res.*, 2019, **52**, 510–519.
14 N. Tamemoto, N. Tamemoto, M. Akishiba, K. Sakamoto, K. Kawano, H. Noguchi and S. Futaki, *Mol. Pharm.*, 2020, **17**, 2175–2185.
15 T. R. Blake, W. C. Ho, C. R. Turlington, X. Zang, M. A. Huttner, P. A. Wender and R. M. Waymouth, *Chem. Sci.*, 2020, **11**, 2951–2966.
16 M. Pazo, M. Juanes, I. Lostalé-Seijo and J. Montenegro, *Chem. Commun.*, 2018, **54**, 6919–6922.
17 M. Pazo, G. Salluce, I. Lostalé-Seijo, M. Juanes, F. Gonzalez, R. Garcia-Fandiño and J. Montenegro, *RSC Chem. Biol.*, 2021, **2**, 503–512.
18 L. Motiei, S. Rahimipour, D. A. Thayer, C. H. Wong and M. R. Ghadiri, *Chem. Commun.*, 2009, 3693–3695.
19 N. G. Bednarska, B. W. Wren and S. J. Willcocks, *Drug Discov. Today*, 2017, **22**, 919–926.
20 E. González-Freire, F. Novelli, A. Pérez-Estévez, R. Seoane, M. Amorín and J. R. Granja, *Chem. - A Eur. J.*, 2021, **27**, 3029–3038.
21 L. Dutot, P. Lécorché, F. Burlina, R. Marquant, V. Point, S. Sagan, G. Chassaing, J.-M. Mallet and S. Lavielle, *J. Chem. Biol.*, 2010, **3**, 51–65.
22 P. Morelli, E. Bartolami, N. Sakai and S. Matile, *Helv. Chim. Acta*, 2018, **101**, e1700266.
23 I. Gallego, A. Rioboo, J. J. Reina, B. Díaz, Á. Canales, F. J. Cañada, J. Guerra-Varela, L. Sanchez and J. Montenegro, *ChemBioChem*, 2019, **20**, 1400–1409.
24 P. Lécorché, A. Walrant, F. Burlina, L. Dutot, S. Sagan, J.-M. Mallet, B. Desbat, G. Chassaing, I. D. Alves and S. Lavielle, *Biochim. Biophys. Acta-Biomembranes*, 2012, **1818**, 448–457.
25 S. Kawakami and M. Hashida, *J. Control. Release*, 2014, **190**, 542–555.
26 I. Lostalé-Seijo, I. Louzao, M. Juanes and J. Montenegro, *Chem. Sci.*, 2017, **8**, 7923–7931.
27 A. Fuertes, J. Marisa, J. R. Granja and J. Montenegro, *Chem. Commun.*, 2017, **53**, 7861–7871.
28 M. Juanes, I. Lostalé-Seijo, J. R. Granja and J. Montenegro, *Chem. - A Eur. J.*, 2018, **24**, 10689–10698.
29 A. Méndez-Ardoy, J. J. Reina and J. Montenegro, *Chem. - A Eur. J.*, 2020, **26**, 7516–7536.
30 J. J. Reina, A. Rioboo and J. Montenegro, *Synth.*, 2018, **50**, 831–845.
31 M. Hällbrink, J. Oehlke, G. Papsdorf and M. Bienert, *Biochim. Biophys. Acta - Biomembr.*, 2004, **1667**, 222–228.